



**HAL**  
open science

# The Unexpected Helical Supramolecular Assembly of a Simple Achiral Acetamide Tecton Generates Selective Water Channels

Dan Dumitrescu, Jordi Rull-Barull, Anthony R. Martin, Nathalie Masquelez, Maurizio Polentarutti, Annie Heroux, Nicola Demitri, Giorgio Bais, Ionut-Tudor Moraru, Romuald Poteau, et al.

► **To cite this version:**

Dan Dumitrescu, Jordi Rull-Barull, Anthony R. Martin, Nathalie Masquelez, Maurizio Polentarutti, et al.. The Unexpected Helical Supramolecular Assembly of a Simple Achiral Acetamide Tecton Generates Selective Water Channels. *Chemistry - A European Journal*, 2022, 28 (33), pp.e202200383. 10.1002/chem.202200383 . hal-03643372v2

**HAL Id: hal-03643372**

**<https://hal.science/hal-03643372v2>**

Submitted on 21 Oct 2022

**HAL** is a multi-disciplinary open access archive for the deposit and dissemination of scientific research documents, whether they are published or not. The documents may come from teaching and research institutions in France or abroad, or from public or private research centers.

L'archive ouverte pluridisciplinaire **HAL**, est destinée au dépôt et à la diffusion de documents scientifiques de niveau recherche, publiés ou non, émanant des établissements d'enseignement et de recherche français ou étrangers, des laboratoires publics ou privés.



Distributed under a Creative Commons Attribution 4.0 International License

WILEY-VCH

 **Chemistry  
Europe**

European Chemical  
Societies Publishing

# Take Advantage and Publish Open Access



By publishing your paper open access, you'll be making it immediately freely available to anyone everywhere in the world.

That's maximum access and visibility worldwide with the same rigor of peer review you would expect from any high-quality journal.

**Submit your paper today.**



[www.chemistry-europe.org](http://www.chemistry-europe.org)



# The Unexpected Helical Supramolecular Assembly of a Simple Achiral Acetamide Tecton Generates Selective Water Channels

Dan G. Dumitrescu,<sup>[a]</sup> Jordi Rull-Barull,<sup>[b]</sup> Anthony R. Martin,<sup>[b]</sup> Nathalie Masquelez,<sup>[c]</sup> Maurizio Polentarutti,<sup>[a]</sup> Annie Heroux,<sup>[a]</sup> Nicola Demitri,<sup>[a]</sup> Giorgio Bais,<sup>[a]</sup> Ionut-Tudor Moraru,<sup>[d, e]</sup> Romuald Poteau,<sup>[e]</sup> Muriel Amblard,<sup>[b]</sup> Andraž Krajnc,<sup>[f]</sup> Gregor Mali,<sup>[f]</sup> Yves-Marie Legrand,<sup>[g]</sup> Arie van der Lee,<sup>\*[c]</sup> and Baptiste Legrand<sup>[b]</sup>

**Abstract:** Achiral 2-hydroxy-*N*-(diphenylmethyl)acetamide (HNDPA) crystallizes in the  $P6_1$  chiral space group as a hydrate, building up permeable chiral crystalline helical water channels. The crystallization-driven chiral self-resolution process is highly robust, with the same air-stable crystalline form readily obtained under a variety of conditions. Interestingly, the HNDPA supramolecular helix inner pore is filled by a helical water wire. The whole edifice is mainly stabilized by robust hydrogen bonds involving the HNDPA amide bonds and  $\text{CH}\cdots\pi$  interactions between the HNDPA phenyl groups.

The crystalline structure shows breathing behavior, with completely reversible release and re-uptake of water inside the chiral channel under ambient conditions. Importantly, the HNDPA channel is able to transport water very efficiently and selectively under biomimetic conditions. With a permeability per channel of 3.3 million water molecules per second in large unilamellar vesicles (LUV) and total selectivity against NaCl, the HNDPA channel is a very promising functional nanomaterial for future applications.

## Introduction

Fresh water availability is among the biggest challenges of the 21st century. Nanotechnologies might, one day, provide tools to overcome the shortage of drinkable water. Designing devices able to conduct water molecules in a highly controlled fashion is a very challenging task, mainly because a water molecule is both extremely small and non-ionic.<sup>[1]</sup> Desalination technologies can help mitigate the problem, with several plants already operating in regions of high water stress. The most common method in commercial use is reverse osmosis, and the current

industrial state of the art employs dense polyamide membranes, which in effect “filter” water molecules through random pores too small for solvated ions to pass.<sup>[2]</sup> In spite of recent advances, however, there is an urgent need to improve the processes in operation.<sup>[3,4,5]</sup>

One of the keys to greater separation efficiency lies in controlling the selectivity of water transport at the molecular level, by using well-defined channels with diameters below 3 Å. Nature does this very well, through aquaporins, which are water transporting proteins found in living organisms.<sup>[6]</sup> Their remarkable water transport rates and selectivity are due to the size,

[a] D. G. Dumitrescu, M. Polentarutti, A. Heroux, N. Demitri, G. Bais  
Elettra–Sincrotrone Trieste S.C.p.A.  
Strada Statale 14–km 163,5 in AREA Science Park  
34149 Basovizza, Trieste (Italy)

[b] J. Rull-Barull, A. R. Martin, M. Amblard, B. Legrand  
Institut des Biomolécules Max Mousseron, IBMM  
Université de Montpellier, ENSCM, CNRS  
Montpellier (France)

[c] N. Masquelez, A. van der Lee  
IEM, Université de Montpellier, CNRS, ENSCM  
Montpellier (France)  
E-mail: arie.van-der-lee@umontpellier.fr

[d] I.-T. Moraru  
Babes-Bolyai University  
Faculty of Chemistry and Chemical Engineering  
Department of Chemistry  
str. Kogalniceanu, nr. 1, 400084, Cluj-Napoca (Romania)

[e] I.-T. Moraru, R. Poteau  
Université de Toulouse  
INSA, UPS, CNRS; LPCNO (IRSAMC)  
135 avenue de Rangueil, 31077 Toulouse (France)

[f] A. Krajnc, G. Mali  
Department of Inorganic Chemistry and Technology  
National Institute of Chemistry  
Hajdrihova 19, 1001, Ljubljana (Slovenia)

[g] Y.-M. Legrand  
Laboratoire de Chimie Bio-Inspirée et d'Innovations Écologiques  
ChimEco UMR 5021, CNRS  
Université de Montpellier  
Grabels (France)

Supporting information for this article is available on the WWW under <https://doi.org/10.1002/chem.202200383>

© 2022 The Authors. Chemistry - A European Journal published by Wiley-VCH GmbH. This is an open access article under the terms of the Creative Commons Attribution Non-Commercial NoDerivs License, which permits use and distribution in any medium, provided the original work is properly cited, the use is non-commercial and no modifications or adaptations are made.

shape and chemical structure of their internal channels, which allow water molecules to arrange themselves and travel in ordered “water wires”, excluding ions and protons in the process.<sup>[7]</sup> Most of current research is focused on mimicking this strategy by designing artificial water permeable pores with well-defined structure and chemistry.<sup>[8,9]</sup> One possible strategy is to use large chemical objects, such as carbon nanotubes<sup>[10,11,12]</sup> or graphene oxide.<sup>[13,14]</sup> Other studies rely however on the arrangement of small molecules into larger porous supramolecular entities.<sup>[15]</sup> This allows for more structural flexibility, as the shape and nature of the building tectons direct the self-assembly process to create functional nanomaterials.<sup>[16]</sup> Molecular tectons with a central cavity can stack themselves into continuous porous tubules, as is the case of calixarene<sup>[17,18]</sup> and pillarene derivatives.<sup>[19]</sup>

The most promising approaches take inspiration from nature, relying on robust and directional amide hydrogen bond motifs. Some of the earliest examples are tubular oligopeptide structures which reversibly accommodates various solvent molecules.<sup>[20]</sup> It was shown that by varying the oligopeptide structure and length, one can facilitate the formation of water wires.<sup>[21,22]</sup> Both discrete<sup>[23,24]</sup> and polymeric<sup>[25]</sup> metal complexes were also successfully employed for stabilizing water wires. Interestingly, in all of these examples, the water wire adopts a helical conformation, and, in some cases, the reversibility of the water transport was also evidenced.<sup>[23]</sup> Barboiu et al. discovered a very simple achiral artificial water channel family, in which imidazole derivatives self-assemble into an I-quartet, forming pores similar to those of natural aquaporins.<sup>[26,27]</sup> Subsequent studies demonstrated their viability in practical desalination applications,<sup>[28,29]</sup> highlighted the effect of using chiral building blocks on water transport directionality, and described a similar system based on diols.<sup>[30]</sup> Helical foldamer channels facilitating selective and fast transport of water and protons have also been reported.<sup>[31,32,33]</sup>

The current discovery starts in this context and is one of serendipity. Milbeo et al. investigated the ability of a highly constrained  $\beta$ -amino acid ((*S*)-aminobicyclo[2.2.2]octane-2-carboxylic acid (H-(*S*)-ABOC-OH) to stabilize families of helical foldamers.<sup>[34]</sup> The ABOC-based oligomers were typically capped by 2-hydroxy-*N*-(diphenylmethyl)acetamide esters, also known as *N*-benzhydryl-glycolamide esters, or OBg esters.<sup>[35,36]</sup> During the crystallization process from methanol, some of them underwent transesterification, resulting in two distinct crystal habits, plates and needles. A single-crystal structure was determined for both types of crystals, where the plates gave the expected helical foldamers, but the needles appeared to be a 2-hydroxy-*N*-(diphenylmethyl)acetamide (HNDPA) hydrate, which was thus a side product of the reaction. Surprisingly, the achiral HNDPA crystallized in a chiral space group forming linear water channels.

In this work, we have explored the characteristics of these artificial water channels by temperature-dependent X-ray diffraction, differential scanning calorimetry (DSC), solid state NMR, density functional calculations, and water transport measurements.

## Results and Discussion

### Synthesis and crystallization

Although the HNDPA hydrate was obtained as a side product, it appears that it is commercially available (CAS 101089-89-8) and that it also could be synthesized by a straightforward one-step reaction, which is a modified version of a previously reported synthesis procedure (Figure 1).<sup>[37]</sup>

Of particular note is the robustness of HNDPA hydrate crystallization, and, by extension, of the chiral self-resolution process. A crystallization assay showed the polymorphic landscape of HNDPA to be unexpectedly barren, with the same chiral hexagonal solid form readily obtained from a wide variety of protic solvents, such as water or water/solvent mixtures, but also from aprotic hydrophobic solvents, such as methylene chloride or ethyl acetate (Table S1 in the Supporting Information). Only traces of water in the solvents and/or scavenging of water molecules from the atmosphere during the crystallization step allow the formation of crystals.

### Structure of HNP A helical water channels

High-resolution single-crystal synchrotron X-ray diffraction was used to determine the structure (Figure S6), as well as to ascertain the chirality of the system. X-ray powder diffraction showed that the bulk material was single-phased (Figure S12). This achiral compound crystallizes in the chiral  $P6_1$  space group, as a 0.4 hydrate with the water molecules arranged in a helical water wire along the *c*-axis (Figure 2). Although not unprecedented, chiral self-resolution is an extremely rare phenomenon, especially in the case of porous structures. Several examples of chiral self-resolution of metal complexes exist,<sup>[38]</sup> mostly involving bulky aromatic ligands. Due to steric overcrowding around the metal center, the achiral ligands become inequivalent, usually resulting in a screw axis in the crystal structure.<sup>[39]</sup> This has been employed in the case of metal–organic frameworks (MOFs), where a small rational increase in the ligand results in a chiral porous structure constructed from achiral materials.<sup>[40]</sup> Chiral self-resolution in organic crystal structures is even rarer, with examples based on 1,3,5-trisubstituted benzene derivatives crystallizing in one of the variants of the enantiomorphic  $P6_1/P6_5$  space group pair.<sup>[41,42]</sup> Other examples are known, all having, curiously, at least an aromatic residue and most often an amide hydrogen bond.<sup>[43,44]</sup>

The water channel, centered along the  $6_1$  screw axis, is comprised of six infinite stacks of HNDPA molecules in the *c*

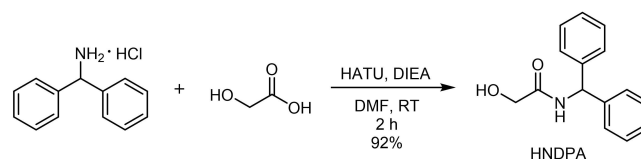
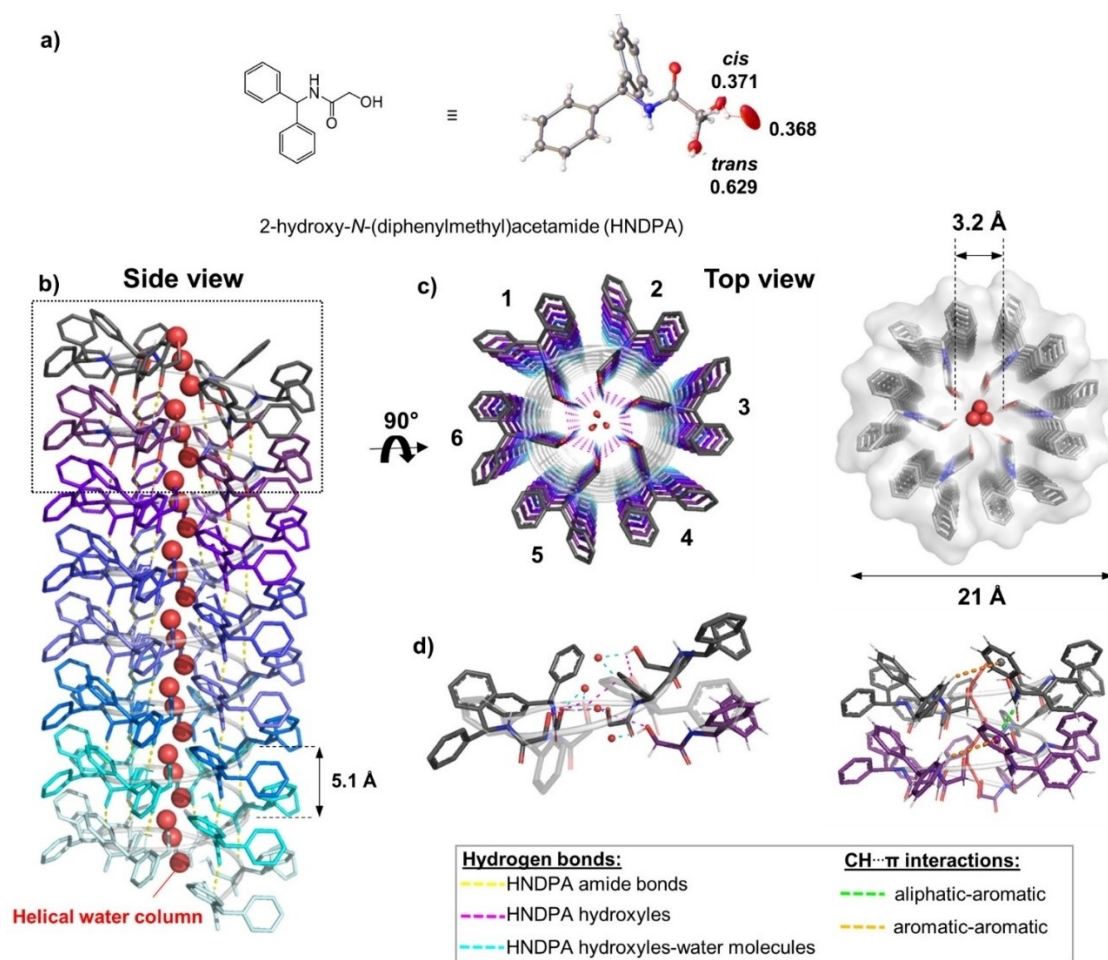


Figure 1. One-step synthesis of HNDPA.



**Figure 2.** a) ORTEP plot of the asymmetric unit, normalized chemical occupancies for oxygen atoms are indicated. b) Side and c) top views of the crystalline water channel. d) Focus on hydrogen bond networks (left) and aromatic and aliphatic-aromatic contacts (right). HNDPA molecules are shown as sticks, water oxygen atoms as red spheres and hydrogen bonds and CH...π interactions as dashed lines.

direction, which form a supramolecular right-handed helix (6 molecules/turn, pitch of 5.1 Å; Figure 2b). The inner channel walls are lined with hydroxy groups, while the hydrophobic diphenyl moieties form the exterior. The channel inner diameter is nearly constant along the *c*-axis, approximately 3.1 Å at 100 K and 3.3 Å at 350 K (Figure 2c). Water molecules inside are slightly disordered along the channel direction having a partial occupancy of around 0.4. The maximum theoretical occupancy would be 0.5 as the  $6_1$  screw axis generates a second channel oxygen at only 2.0 Å from the first one, which is obviously too close to be possible. The reason that the maximum occupancy of 0.5 is not attained is that for this configuration there is still too much steric hindrance for all water molecules to be simultaneously present in the channel. The tentative hydrogen bond network within the channel is shown by red and blue dashed lines in Figure 2d in the hypothesis of a site occupancy factor of 0.5, that is, three water molecules per channel per unit cell.

Lengthwise, the backbone of the structure is stabilized by robust NH...O hydrogen bonds between HNDPA amide bonds (Figure 2b, yellow dashed lines).

This arrangement is further strengthened by CH...π interactions (Figure 2d, green dashed lines) between the tertiary carbon hydrogen and the benzene ring opposite ( $d_{\text{CH}\cdots\text{centroid}} = 2.839$  Å). In the plane perpendicular to the channel direction, the infinite HNDPA stacks are bound together through CH...π contacts between adjacent phenyl groups (Figure 2d, orange dashed lines), as well as through dynamic hydrogen bonds between hydroxy moieties (Figure 2c, d, magenta dashed lines). The OH groups are disordered over two positions, *cis* and *trans* (0.371/0.629 occupancies, Figure 2a). Their putative role in the crystal structure is twofold: providing additional stability through H-bonds between HNDPA molecules, as well as acting as relay points for the water wire inside the channel (minimum distances  $d_{\text{O}_{\text{cis}}\cdots\text{O}_{\text{w}}} = 2.725$  Å and  $d_{\text{O}_{\text{trans}}\cdots\text{O}_{\text{w}}} = 2.657$  Å) and thus facilitating the transport mechanism.

Hydrogen bonds between the HNDPA hydroxy groups and water molecules within the HNDPA supramolecular helix are shown in Figure 2d (cyan dashed lines). The handedness of the helical water channel is defined by the space group:  $P6_1$  corresponds to a *P* helix, and  $P6_5$  to an *M* helix. The structure is comprised entirely of light atoms and therefore the anomalous

signal at high photon energies is too small for discriminating the  $P6_1/P6_5$  space group pair. The absolute structure of the crystal was determined to be in the  $P6_1$  space group, by varying the photon energy and performing a careful likelihood analysis based on Bijvoet differences, showing also that the material is enantiopure. This means that chirality is generated from achiral HNDPA and  $H_2O$  by dissymmetrizing the interactions between them during the crystallization stage. The same type of chirality is present independently of the crystallization solvent used (Table S1) and the channel structure remains intact even when water is released (Figure 3a)

### Temperature-dependent water flow dynamics

Thermogravimetric analysis (TGA) and differential scanning calorimetry (DSC), showed a clear melting point at 365 K, followed by compound degradation at higher temperatures (Figures S13 and S14). The dehydration event could not be observed as a well-defined peak in either mass loss or heating curves, but a small mass loss of about 3% was observed spreading over the whole 303–365 K range, without clear associated thermal event. This is consistent with water release (2.89% mass) being interpreted as a gradual water expulsion from the channel. We tested this hypothesis by studying the release and uptake of water inside the channel using a series of variable temperature single-crystal X-ray diffraction experiments.

These variable temperature studies showed that the crystal-line structure has a breathing-like behavior (Figures 3 and S15–S20). Such behavior is relatively common in MOFs<sup>[45]</sup> and was also observed in some organic cage structures,<sup>[46,47]</sup> but never in organic structures containing helical water channels.

Water is gradually released from the channel at temperatures above 300 K, and reabsorbed from the atmosphere at ambient conditions at 293 K. The water release/uptake is completely reversible, as shown in a series of heating/cooling cycles monitored by diffraction at 10 K temperature intervals, starting at 100 to 350 K and back down (Figure 3a). These cycles were repeated six times on the same crystal, with the sample left in air at 293 K between each cycle. The release of the channel water was tracked by plotting its oxygen occupancy (Figure 3b). The results confirmed the thermogravimetric analysis, as the occupancy remained stable around 0.33 at 310 K, and decreased to low values in the error range, that is, 0.08 occupancy, 25% of the initial water content at the final temperature of 350 K. The release of water is relatively slow because to partially empty the channel the crystal had to be kept for at least 1 h at 350 K. On cooling back to cryogenic temperatures, the water oxygen maintained this low occupancy. Between each cycle, the crystal was able to scavenge water from the atmosphere at room temperature and self-fill to full channel water occupancy in less than 24 h. The data quality, as expressed by the  $R_{\text{int}}$  agreement factor, increased significantly between the first and last temperature cycle, whereas the channel water showed increasingly slower kinetics. We attribute this phenomenon to crystal surface melting just below the

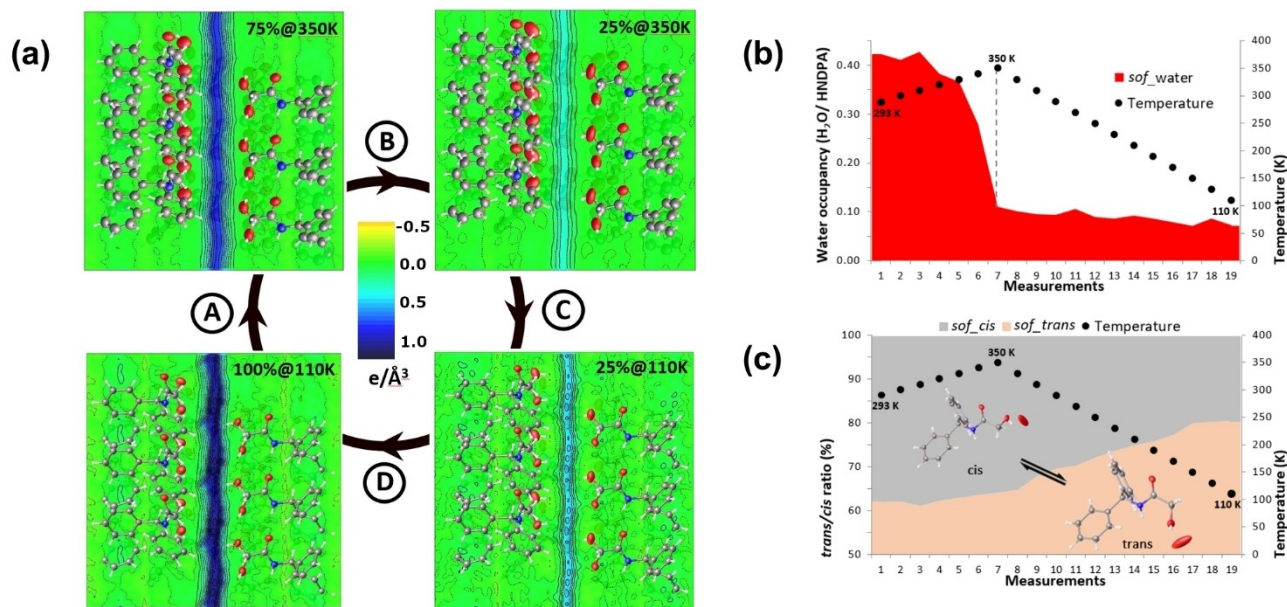


**Figure 3.** Water release–re-uptake cycle and water flow inside the water channel as a function of temperature. a) The panels represent electron density in a lengthwise cross-section of the water channel (front HNDPA molecules have been removed for clarity) with the experimental electron density shown as a color scale [ $e/\text{\AA}^3$ ]; dark blue represents the highest electron density values. The water occupancy is expressed as a percentage with 0.4 considered to be the maximum possible occupancy. (A) Temperature increase from 100 to 350 K; (B) sample left at 350 K for 1 h; (C) temperature decrease at 100 K; (D) sample left at 293 K in air for 24 h and diffraction experiment at 100 K. b) and c) Focus on the water release event (from 293 to 350 K and back to 100 K over 60 min). b) Channel water occupancy and c) *cis/trans* conformation (%), plotted as a function of temperature, expressed by the measurement number. Site occupancy factor (sof) e.s.d.'s are all in the range of 0.005.

melting point. The lower  $R_{\text{int}}$  factor correlates to higher crystallinity, which in turn would entail longer continuous channels and therefore a longer path for the channel water to travel in order to be released. Variable-temperature  $^1\text{H}$  MAS NMR experiments on the crystalline phase between 263 and 343 K, showed a selective narrowing of the water proton signals beyond 303 K (Figure S24). This line narrowing is consistent with an increase of the channel water mobility when the temperature progressively rises to 343 K in agreement with the X-ray study and the thermal analyses.

We were interested in the putative correlation between the water transport and the hydroxy groups flipping motion monitoring the *cis/trans* ratio during the variable temperature single-crystal X-ray diffraction experiments (Figure 3c). Upon heating from 310 to 350 K, water is gradually released from the channels and the *cis/trans* ratio remains stable. When cooling from 350 to 100 K, the water content stays minimum, but the *cis/trans* ratio evolves from 62:38 to 80:20. This behavior was reproducible in all six release–re-uptake cycles. Thus, the hydroxy *trans* conformation is progressively favored over the *cis* when water is released from the channel. Nevertheless, such trend could be simply due to that, when the temperature decreases, most moieties fall in the most stable state, that is, *trans*, as deduced from density functional calculations (Figure S26). Thus, for the moment, the relationship between the discrete flipping motion of HNDPA hydroxy groups and the water mobility in the HNDPA channel remains speculative and should be investigated using further studies such as molecular dynamics.<sup>[48,49]</sup>

### Water transport through lipid bilayers

As was previously shown in the field of new-generation desalination membranes,<sup>[26,27]</sup> transport through lipid bilayers can provide a robust model for further polymeric membranes preparation, such as high-performance polyamide desalination membranes. In order to investigate whether HNDPA channels could promote water transport across bilayers, large unilamellar vesicles (LUVs) were loaded with HNDPA channels and assessed by a stopped-flow method. LUVs were prepared from *Escherichia coli* membrane lipids (Avanti Polar Lipids) and measurements performed at 20 °C. A lipid-to-channel ratio (LCR) of 50 was used. As negative reference, we synthesized 2-hydroxy-*N*-(phenylmethyl)acetamide (HNPA), a close analogue of HNDPA but with a single phenyl ring. Based on the structural features of the HNDPA self-assembly, we hypothesized that HNPA can no longer stack to form channels. Indeed, the HNPA does not have a columnar rosette-like structure as HNDPA in the crystal, but rather a achiral columnar structure arranged in sheets where the hydroxy groups are hydrogen bonded to the amine and carbonyl groups of neighboring columns, without any water containing channel (Figures 4, S30 and S31). The net permeability was 8.3 and 0.4  $\mu\text{m s}^{-1}$  for HNDPA-LUV and HNPA-LUV, respectively (Figure S27). The water permeability per channel  $P_c$  was also calculated for HNDPA and turned out to be  $P_c = 9.7 \times 10^{-17} \text{ cm}^3 \text{ s}^{-1}$ , which can also be expressed as  $P_{\text{ws}} =$

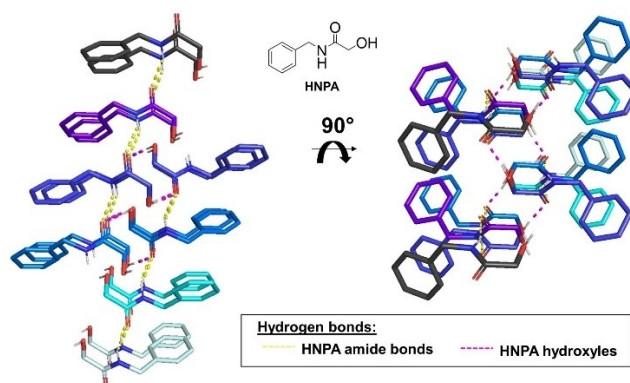


Figure 4. X-ray structure of the negative reference compound HNPA.

$3.3 \times 10^6$  water molecules per second (see the Supporting Information for details) for LCR=50. In addition, the ions permeability was tested for HNDPA in order to control if sodium was transported together with water. For this, a 200 mM NaCl shock solution (Figure S28) was used to induce ion transport but no significant difference could be measured with the reference LUVs. Importantly, compared to previously reported artificial water channels, the net permeability and the selectivity of HNDPA channels for water are very high.<sup>[50]</sup> This apparent total salt exclusion for an artificial self-assembled water channels is rare enough to be highlighted. Such water transport and selectivity in presence of HNDPA could be due to the formation well-defined self-assembled channels and not to a potential destabilization of the lipid bilayers.

### Conclusion

We unexpectedly found a simple tecton able to self-assemble into a robust water-channel structure in the solid state, stabilized by a strong intermolecular interaction network. HNDPA molecules form a supramolecular helix whose inner pore is filled by a helical water wire. The HNDPA channel is functional and is among the most permeable and selective artificial channels for water when inserted into LUVs in the presence of NaCl. Based on these surprising results, we are currently enlarging this new artificial water channel family by synthesizing HNDPA derivatives. In addition, to gain new insights into the self-assembly of these simple tectons, research is ongoing towards tentatively optimizing their properties. Such easy-to-make artificial water channels could be employed for selectively promoting water transport in polymeric membranes; something that still constitutes a great challenge.

### Experimental Section

Deposition Numbers 1960786–1960790 (for HNDPA) and 2142860 (for HNPA) contain the supplementary crystallographic data for this paper. These data are provided free of charge by the joint

Cambridge Crystallographic Data Centre and Fachinformationszentrum Karlsruhe Access Structures service.

## Acknowledgements

The authors acknowledge the CERIC-ERIC Consortium for the access to experimental facilities and financial support. We thank the CNRS and the Université de Montpellier for financial support. We also thank the LMP (Laboratoire de Mesures Physiques) for providing access to EA and NMR facilities. The authors thank Lionel Verdoucq (UMR BPMP, Montpellier, France) for useful help and advices related to the stopped-flow measurements and Eddy Petit (IEM, Montpellier, France) is thanked for carrying out the infrared spectroscopy measurements.

## Conflict of Interest

The authors declare no conflict of interest.

## Data Availability Statement

The data that support the findings of this study are available from the corresponding author upon reasonable request.

**Keywords:** chirality · crystal engineering · helices · water channels · water transport

- [1] Organisation des Nations Unies pour l'éducation, *The United Nations World Water Development Report 2019*, United Nations, 2019.
- [2] M. Qasim, M. Badrelzaman, N. N. Darwish, N. A. Darwish, N. Hilal, *Desalination* 2019, 459, 59–104.
- [3] H. B. Park, J. Kamcev, L. M. Robeson, M. Elimelech, B. D. Freeman, *Science* 2017, 356, eaab0530.
- [4] R. Li, L. Zhang, P. Wang, *Nanoscale* 2015, 7, 17167–17194.
- [5] J. R. Werber, C. O. Osuji, M. Elimelech, *Nat. Rev. Mater.* 2016, 1, 16018.
- [6] P. Agre, *Angew. Chem. Int. Ed.* 2004, 43, 4278–4290; *Angew. Chem.* 2004, 116, 4377–4390.
- [7] U. Kosinska Eriksson, G. Fischer, R. Friemann, G. Enkavi, E. Tajkhorshid, R. Neutze, *Science* 2013, 340, 1346–1349.
- [8] M. Barboiu, A. Gilles, *Acc. Chem. Res.* 2013, 46, 2814–2823.
- [9] W. Song, M. Kumar, *Curr. Opin. Chem. Eng.* 2019, 25, 9–17.
- [10] Ihsanullah, *Sep. Purif. Technol.* 2019, 209, 307–337.
- [11] J. Wu, K. Gerstandt, H. Zhang, J. Liu, B. J. Hinds, *Nat. Nanotechnol.* 2012, 7, 133–139.
- [12] H. Tunuguntla Ramya, Y. Henley Robert, Y.-C. Yao, A. Pham Tuan, M. Wanunu, A. Noy, *Science* 2017, 357, 792–796.
- [13] S. Homaeigohar, M. Elbahri, *NPG Asia Mater.* 2017, 9, e427–e427.
- [14] H. Huang, Z. Song, N. Wei, L. Shi, Y. Mao, Y. Ying, L. Sun, Z. Xu, X. Peng, *Nat. Commun.* 2013, 4, 2979.
- [15] I. Kocsis, Z. Sun, Y. M. Legrand, M. Barboiu, *npj Clean Water* 2018, 1, 1–11.
- [16] E. Busseron, Y. Ruff, E. Moulin, N. Giuseppone, *Nanoscale* 2013, 5, 7098–7140.
- [17] A. W. Coleman, E. D. Silva, F. Nouar, M. Nierlich, A. Navaza, *Chem. Commun.* 2003, 826–827.
- [18] P. K. Thallapally, G. O. Lloyd, J. L. Atwood, L. J. Barbour, *Angew. Chem. Int. Ed.* 2005, 44, 3848–3851; *Angew. Chem.* 2005, 117, 3916–3919.
- [19] X.-B. Hu, Z. Chen, G. Tang, J.-L. Hou, Z.-T. Li, *J. Am. Chem. Soc.* 2012, 134, 8384–8387.
- [20] C. H. Görbitz, *Acta Crystallogr. Sect. B* 2002, 58, 849–854.
- [21] U. S. Raghavender, S. Aravinda, N. Shamala, R. Rai, P. Balam, *J. Am. Chem. Soc.* 2009, 131, 15130–15132.
- [22] U. S. Raghavender, Kantharaju, S. Aravinda, N. Shamala, P. Balam, *J. Am. Chem. Soc.* 2010, 132, 1075–1086.
- [23] A. Mukherjee, M. K. Saha, M. Nethaji, A. R. Chakravarty, *Chem. Commun.* 2004, 716.
- [24] Z. Fei, D. Zhao, T. J. Geldbach, R. Scopelliti, P. J. Dyson, S. Antonijevic, G. Bodenhausen, *Angew. Chem. Int. Ed.* 2005, 44, 5720–5725; *Angew. Chem.* 2005, 117, 5866–5871.
- [25] B. Sreenivasulu, J. J. Vittal, *Angew. Chem. Int. Ed.* 2004, 43, 5769–5772; *Angew. Chem.* 2004, 116, 5893–5896.
- [26] Y. Le Duc, M. Michau, A. Gilles, V. Gence, Y.-M. Legrand, A. van der Lee, S. Tingry, M. Barboiu, *Angew. Chem. Int. Ed.* 2011, 50, 11366–11372; *Angew. Chem.* 2011, 123, 11568–11574.
- [27] I. Kocsis, M. Sorci, H. Vanselow, S. Murail, S. E. Sanders, E. Licsandru, Y.-M. Legrand, A. van der Lee, M. Baaden, P. B. Petersen, G. Belfort, M. Barboiu, *Sci. Adv.* 2018, 4, eaao5603.
- [28] M. Di Vincenzo, A. Tiraferri, V.-E. Musteata, S. Chisca, R. Sougrat, L.-B. Huang, S. P. Nunes, M. Barboiu, *Nat. Nanotechnol.* 2020, 16, 190–196.
- [29] L. B. Huang, M. Di Vincenzo, Y. Li, M. Barboiu, *Chem. Eur. J.* 2021, 27.
- [30] L.-B. Huang, A. Hardiagon, I. Kocsis, C.-A. Jegu, M. Deleanu, A. Gilles, A. van der Lee, F. Sterpone, M. Baaden, M. Barboiu, *J. Am. Chem. Soc.* 2021, 143, 4224–4233.
- [31] J. Shen, J. Fan, R. Ye, N. Li, Y. Mu, H. Zeng, *Angew. Chem. Int. Ed.* 2020, 59, 13328–13334; *Angew. Chem.* 2020, 132, 13430–13436.
- [32] J. Shen, R. Ye, A. Romanies, A. Roy, F. Chen, C. Ren, Z. Liu, H. Zeng, *J. Am. Chem. Soc.* 2020, 142, 10050–10058.
- [33] A. Roy, J. Shen, H. Joshi, W. Song, Y.-M. Tu, R. Chowdhury, R. Ye, N. Li, C. Ren, M. Kumar, A. Aksimentiev, H. Zeng, *Nat. Nanotechnol.* 2021, 16, 911–917.
- [34] P. Milbeo, J. Martinez, M. Amblard, M. Calmès, B. Legrand, *Acc. Chem. Res.* 2021, 54, 685–696.
- [35] B. Legrand, C. André, E. Wenger, C. Didierjean, M. C. Averlant-Petit, J. Martinez, M. Calmes, M. Amblard, *Angew. Chem. Int. Ed.* 2012, 51, 11267–11270; *Angew. Chem.* 2012, 124, 11429–11432.
- [36] C. André, B. Legrand, L. Moulat, E. Wenger, C. Didierjean, E. Aubert, M. C. Averlant-Petit, J. Martinez, M. Amblard, M. Calmes, *Chem. Eur. J.* 2013, 19, 16963–16971.
- [37] L. S. Zamudio Rivera, L. Carrillo, T. Mancilla, *Org. Prep. Proc. Intl.* 2000, 32, 84–88.
- [38] L. Pérez-García, D. B. Amabilino, *Chem. Soc. Rev.* 2002, 31, 342–356.
- [39] I. Katsuki, Y. Motoda, Y. Sunatsuki, N. Matsumoto, T. Nakashima, M. Kojima, *J. Am. Chem. Soc.* 2002, 124, 629–640.
- [40] J.-T. Yu, Y.-Y. Shi, J. Sun, J. Lin, Z.-T. Huang, Q.-Y. Zheng, *Sci. Rep.* 2013, 3.
- [41] R. A. Gossage, E. Muñoz-Martínez, H. Frey, A. Burgath, M. Lutz, A. L. Spek, G. van Koten, *Chem. Eur. J.* 1999, 5, 2191–2197.
- [42] I. Azumaya, D. Uchida, T. Kato, A. Yokoyama, A. Tanatani, H. Takayanagi, T. Yokozawa, *Angew. Chem. Int. Ed.* 2004, 43, 1360–1363; *Angew. Chem.* 2004, 116, 1384–1387.
- [43] A. Bajpai, P. Venugopalan, J. N. Moorthy, *CrystEngComm* 2014, 16, 4853–4860.
- [44] X. Shang, I. Song, G. Y. Jung, W. Choi, H. Ohtsu, J. H. Lee, J. Y. Koo, B. Liu, J. Ahn, M. Kawano, S. K. Kwak, J. H. Oh, *Nat. Commun.* 2018, 9.
- [45] M. W. Logan, S. Langevin, Z. Xia, *Sci. Rep.* 2020, 10, 1492.
- [46] T. Hasell, M. Schmidtman, C. A. Stone, M. W. Smith, A. I. Cooper, *Chem. Commun.* 2012, 48, 4689–4691.
- [47] M. Liu, L. Chen, S. Lewis, S. Y. Chong, M. A. Little, T. Hasell, I. M. Aldous, C. M. Brown, M. W. Smith, C. A. Morrison, L. J. Hardwick, A. I. Cooper, *Nat. Commun.* 2016, 7, 12750.
- [48] C. I. Lynch, S. Rao, M. S. P. Sansom, *Chem. Rev.* 2020, 120, 10298–10335.
- [49] D. R. Barden, H. Vashisth *Front. Chem.* 2021, 9, 890.
- [50] E. Licsandru, I. Kocsis, Y.-x. Shen, S. Murail, Y.-M. Legrand, A. van der Lee, D. Tsai, M. Baaden, M. Kumar, M. Barboiu, *J. Am. Chem. Soc.* 2016, 138, 5403–5409.

Manuscript received: February 8, 2022

Accepted manuscript online: April 14, 2022

Version of record online: [REDACTED]